ELSEVIER

Journal of Nuclear Materials 275 (1999) 231–245

journal of nuclear materials

www.elsevier.nl/locate/jnucmat

Review

Fluorination of uranium dioxide particles: a review of physical and chemical properties of the compounds involved

S.S. Sazhin[a,*], A.P. Jeapes[b]

[a] *School of Engineering, Faculty of Science and Engineering, University of Brighton, Cockcroft Building, Lewes Road, Brighton BN2 4GL, UK*

[b] *BNFL, Sellafield, Seaside, Cumbria CA20 1PG, UK*

Received 26 June 1998; accepted 18 May 1999

Abstract

A review of literature related to the process of fluorination of uranium dioxide and physical properties of the compounds involved (uranium hexafluoride, fluorine, uranium dioxide and argon) is presented. It is pointed out that there exist strong indications that the maximum rate of fluorination of uranium dioxide can be achieved at temperatures above 540°C. Particular attention is focused on the study of transport properties of argon–fluorine plasma.

1. Introduction

The aim of this paper is to provide a review of literature related to the process of fluorination of uranium dioxide and physical properties of the elements involved. Some results of this review were implicitly used in the numerical modelling of the fluorination process as reported by Sazhin and Jeapes [1].

The reaction of fluorine and uranium dioxide leading to the production of uranium hexafluoride has been extensively studied for many years [2,3]. These studies, however, have so far been restricted to temperatures below 540°C, indicating that the rate of reaction at temperatures close to 540°C increases rather rapidly with increasing temperature. One might assume that this increase of reaction rate with temperature will continue at temperatures beyond 540°C. This, in its turn, suggests that heating uranium dioxide to temperatures above 540°C may achieve a considerable increase in the rate of production of uranium hexafluoride. At these temperatures, however, the medium becomes highly ionized and turns into the uranium–fluorine plasma. The properties of this plasma will also be covered in the review.

A brief review of studies of the fluorination of uranium dioxide is presented in Section 2. In Sections 3–5 we discuss the main physical properties of the compounds taking part in this reaction or produced as its products (UO_2, UF_6 and F_2) as well as argon which is used in the discharge process. The reported properties of uranium–fluorine plasma are discussed in Section 6. In Section 7 we give a brief overview of particulate dynamics which might be useful when uranium dioxide takes part in the reaction process in the form of aerosols or powder. The main results of this paper are summarised in Section 8.

2. Chemical reaction

The kinetics of fluorination of uranium dioxide by fluorine were studied experimentally by Yahata and Iwasaki [4], Sakurai [3] (UO_2 powder) and Iwasaki [2] (UO_2 pellets). In what follows we will concentrate on the latter paper, as it provides data at the highest reported temperature and gives a useful introduction to the problem. The conclusions of this paper will be compared with those of Sakurai [3] where appropriate.

The process of fluorination of uranium dioxide can be subdivided into two main steps. Firstly

$$UO_2 + F_2 \rightarrow UO_2F_2 \tag{2.1}$$

* Corresponding author.

0022-3115/99/$ - see front matter
PII: S0022-3115(99)00131-2

(chemisorption of fluorine), secondly

$$UO_2F_2 + 2F_2 \rightarrow UF_6 + O_2. \quad (2.2)$$

In the case of UO_2 pellets, Iwasaki [2] separates the process:

$$UO_2 \text{ (pellets)} \rightarrow UO_2 \text{ (partly fluorinated powder)} \quad (2.3)$$

which precedes the reaction (2.1) forming UO_2F_2 powder.

The combined reaction (2.1) and (2.2) is accompanied by a heat release of 244.5 kcal/mol [5].

Processes (2.3) and (2.2) are surface reactions which proceed at the interface between the pellet core and the intermediate layer (partly fluorinated UO_2F_2 powder) and on the outside of this intermediate layer respectively, whereas process (2.1) proceeds throughout the intermediate layer.

At temperatures below 430°C the rate of reaction (2.2) is negligibly small, so that the fluorination results in the production of UO_2F_2 powder only. No experiments were performed by Iwasaki [2] at temperatures below 300°C, where the reaction proceeds very slowly. Above 430°C the rate of reaction (2.2) increases and the quantity of the intermediate UO_2F_2 powder begins to reduce.

UO_2 pellets used in Iwasaki's [2] experiment were 2 mm thick, 6 mm diameter and 10.53 ± 0.11 g/cm^3 average density. The concentration of F_2 varied from 10 to 40 vol.%.

Plots of weight loss of pellets per unit area versus time for F_2 concentration 20 vol.% and different temperatures in the range from 460°C to 540°C are shown in Fig. 1. As follows from this figure, this weight loss is almost a linear function of time which allows us to use the concept of constant rate of reaction at the surface of UO_2 pellets. This reaction rate increases with increasing temperature up to $T = 540$°C. No observations were performed above this temperature.

The reaction rates, k, calculated from Fig. 1 are shown in Table 1 in units of g/(cm^2 h) and mm/h. Note that

$$k\left(\frac{\text{mm}}{\text{h}}\right) = \frac{10}{\rho_{UO_2}} k\left(\frac{\text{g}}{\text{cm}^2\,\text{h}}\right) \approx 0.95k\left(\frac{\text{g}}{\text{cm}^2\,\text{h}}\right). \quad (2.4)$$

The plot of $\log(k(\text{mm/h}) \times 10^2)$ versus $1/T(\text{K}) \times 10^3$, based on Table 1, is shown in Fig. 2. This data suggests that $\log k$ is approximately proportional to $1/T$, which agrees with the Arrhenius law for the reaction rate [6]. Considering temperatures higher than 540°C $\approx$ 813 K, we can extrapolate the line in Fig. 2 towards lower values of $1/T$ but we cannot say at the moment how far this extrapolation can go.

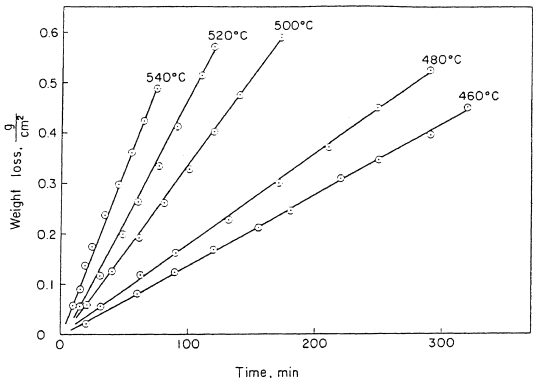

Fig. 1. Weight loss per unit surface of pellet at different temperatures and fluorine concentration 20 vol.%. The gas flow rate was 20 l/h (the reaction was not much affected by the gas flow rate at this level of flow). Reprinted from Journal of Nuclear Materials, volume 25, paper by M. Iwasaki, Kinetics of the fluorination of uranium dioxude pellets by fluorine, pp. 216–226, Fig. 6 [2], Copyright (1968), with permission from Elsevier Science.

Table 1
Experimental reaction rate constants

Temperature (°C)	k (mm/h)	k (g/cm^2 h)
460	0.081	0.085
480	0.104	0.109
500	0.200	0.210
520	0.278	0.292
540	0.380	0.400

Plots of weight loss of pellets per unit area versus time for the temperature 480°C and different concentrations of F_2 are shown in Fig. 3. It follows from this figure, below 12% fluorine, the plots in Fig. 3 deviate from a linear relationship. This deviation from linearity is reflected in the shaded area of Fig. 4 where the plot of the reaction rate (in (g/cm^2 h)) versus volume percent of F_2 is presented. When the concentration of F_2 is larger than 20% but below 40% then the reaction rate is an almost linear function of F_2 volume concentration. No data was reported by Iwasaki [2] for F_2 volume concentrations above 40%.

It is interesting to compare the reaction rates presented in Table 1 and those reported by Sakurai [3] for the reaction of F_2 with UO_2 powder. The reaction rate of F_2 with UO_2 powder with initial weight 100mg and concentration of F_2 20 vol.% (152 mm Hg) as a function of temperature is shown in Fig. 5. Taking a temperature $T = 500$°C we see from Fig. 5 that the reaction rate for this temperature is approximately equal to 0.016 g/min. This means that the relative change of weight of UO_2 powder in the experiment reported by Sakurai [3] is

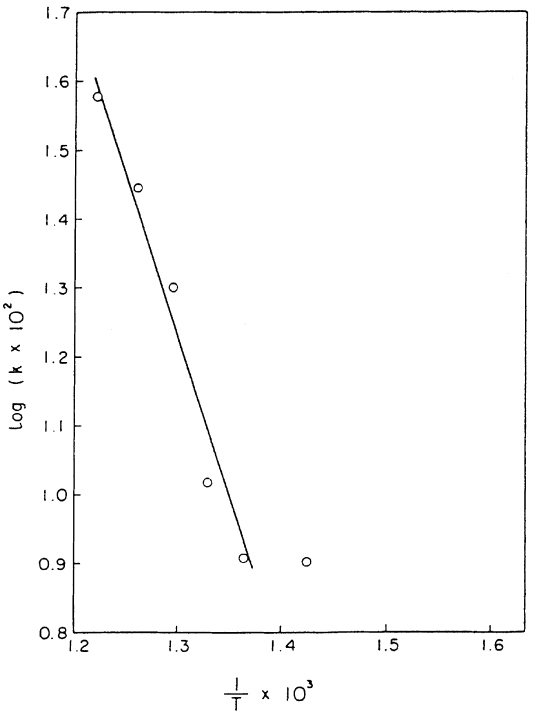

Fig. 2. Effect of temperature on the reaction rate in mm/h for temperatures in the range from 460°C to 540°C (note that the temperature in this figure is measured in K) Fluorine concentration 20 vol.% and the gas flow rate was 20 l/h as in Fig. 1. Reprinted from Journal of Nuclear Materials, volume 25, paper by M. Iwasaki, Kinetics of the fluorination of uranium dioxude pellets by fluorine, pp. 216–226, Fig. 8 [2], Copyright (1968), with permission from Elsevier Science.

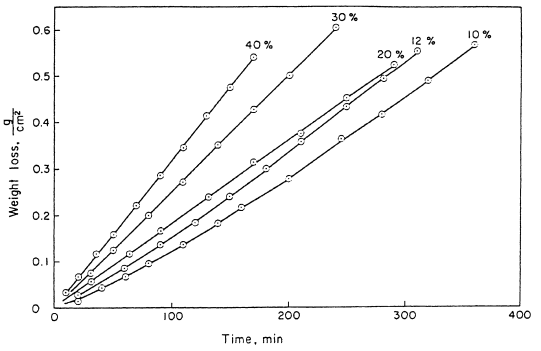

Fig. 3. Effect of fluorine concentration on weight loss per unit surface of pellet at different fluorine concentrations. The temperature was taken 480°C. The gas flow rate was 20 l/h as in Fig. 1. Partially reprinted from Journal of Nuclear Materials, vol. 25, paper by M. Iwasaki, Kinetics of the fluorination of uranium dioxude pellets by fluorine, pp. 216–226, Fig. 5 [2], Copyright (1968), with permission from Elsevier Science.

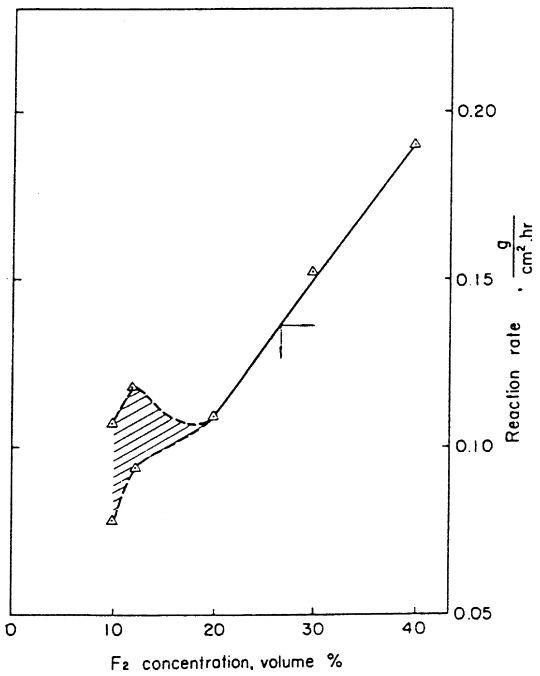

Fig. 4. Effect of fluorine concentration on reaction rate. The temperature was taken 480°C. The gas flow rate was 20 l/h as in Fig. 1. This figure is a partial reproduction of Fig. 4 by Iwasaki [2], Copyright (1968), with permission from Elsevier Science.

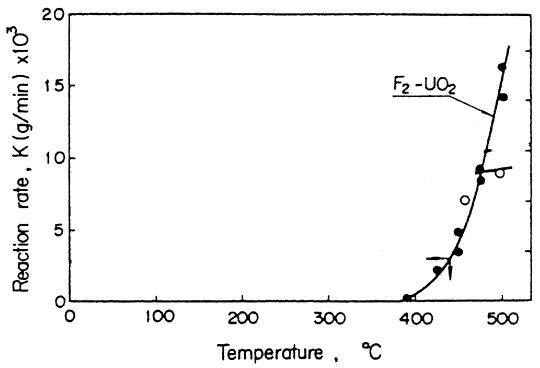

Fig. 5. Temperature dependence of the rate of reaction with the initial weight of UO_2 100 mg. F_2 partial pressure 152 mm Hg. The carrier gas was helium. This figure is a partial reproduction of Fig. 3 by Sakurai [3], Copyright (1974), with permission from American Chemical Society.

$$k_{\text{rel (Sakurai)}} \approx \frac{0.016\ \text{g/min}}{0.1\ \text{g}} = 0.16\frac{1}{\text{min}}. \tag{2.5}$$

At the same time, from Table 1 we obtain the relative change of weight of UO_2 pellets for the same temperature 500°C

$$k_{\text{rel (Iwasaki)}} = \frac{0.211\left(\pi D_{\text{pel}} h_{\text{pel}} + \pi D_{\text{pel}}^2/4\right)}{\rho_{UO_2}\left(\pi D_{\text{pel}}^2 h_{\text{pel}}/4\right)60} \approx 0.004\frac{1}{\text{min}}, \quad (2.6)$$

where D_{pel} and h_{pel} are diameter and height of UO_2 pellets (equal to 0.6 and 0.2 cm, respectively), ρUO_2 is the density of UO_2 pellets (equal to 10.53 g/cm^3).

Comparing (2.5) and (2.6) we can see that k_{rel} for powder is about 40 times greater than k_{rel} for pellets, which can be mainly attributed to the increased surface area of the powder (the average size of powder particles was not specified). The contribution of other effects (e.g., turbulence: see Magnussen and Hjertager [7]) also needs to be explored.

Sakurai [3] also reported the dependence of reaction rate on the carrier gas. At a temperature of 450°C the change from helium to argon or nitrogen resulted in a decrease of reaction rate by nearly a half. At higher temperatures, however, e.g., 475°C, the reaction proceeded more rapidly in argon than in helium at the initial stage, and argon maintains higher temperatures for a considerably longer time than helium (see Fig. 6). The reaction in argon then eventually slows down as the temperature returns to the original line (475°C).

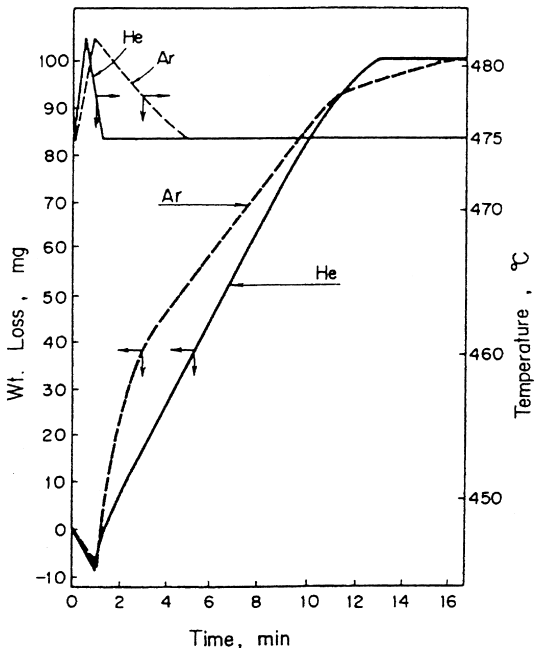

Fig. 6. Changes in weight and temperature during F_2–OU_2 reactions at 475 C in different dilutants of F_2 helium and argon; initial weight of UO_2 100 mg. F_2 partial pressure 152 mm Hg. Reprinted with permission from Fig. 4 by Sakurai [3], Copyright (1974), American Chemical Society.

3. Physical properties of UO_2

Since the preparation of this review, data relevant to density of UO_2, its thermal conductivity, enthalpy and heat capacity have been collected in three review papers prepared at the International Nuclear Safety Center (INSC) at Argonne National Laboratory (see their web pages: http://www.insc.anl.gov/matprop/uo2/density/solid/soldens.html, http://www.insc.anl.gov/matprop/uo2/cond/kuo2s.html, http://www.insc.anl.gov/matprop/uo2/ent_hc//solid//hcp.html). This results in some overlap between the appropriate sections of this review and the INSC reviews, but our approaches are certainly not identical.

3.1. Density

The density of UO_2 at room temperature (15–20°C) is [8]

$$\rho_{UO_2} = 10900 \text{ kg/m}^3. \quad (3.1)$$

This value might be slightly different based on other sources. Say, CRC Handbook of Chemistry and Physics [9] gives the value of $\rho_{UO_2} = 10960$ kg/m^3. The latter value is recommended by INSC.

At higher temperatures these values of density are affected by thermal expansion which was extensively studied by Martin [10]. He suggested that for stoichiometric UO_2 this expansion can be described by the following expressions

$$L = L_{273}\left(9.9734 \times 10^{-1} + 9.802 \times 10^{-6}T - 2.705 \times 10^{-10}T^2 + 4.391 \times 10^{-13}T^3\right) \quad (3.2)$$

for

$$273 \text{ K} \leqslant T \leqslant 923 \text{ K}$$

and

$$L = L_{273}\left(9.9672 \times 10^{-1} + 1.179 \times 10^{-5}T - 2.429 \times 10^{-9}T^2 + 1.219 \times 10^{-12}T^3\right) \quad (3.3)$$

for

$$923 \text{ K} \leqslant T \leqslant 3120 \text{ K (melting point)},$$

where L and L_{273} are lengths at a temperature of T (K) and 273 K, respectively.

The density at 273 K is taken equal to 10963 kg/m^3.

Agreement between expressions (3.2) and (3.3) with available experimental data is illustrated in Fig. 7. As can be seen from this figure, the value of L near the melting point can increase by about 4% which corresponds to the reduction of ρ_{UO_2} by about 12%, which will have to be accounted for in practical computations.

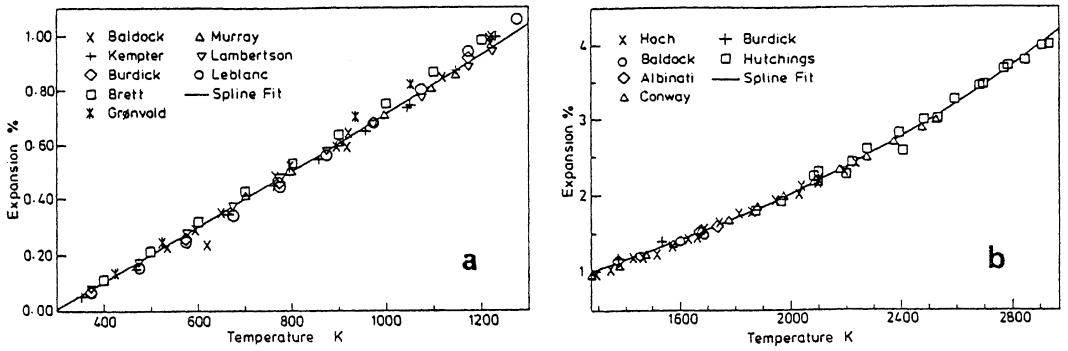

Fig. 7. A fit of the preferred UO_2 thermal expansion data to cubic splines (Eqs. (3.2) and (3.3)). Reprinted from Journal of Nuclear Materials, vol. 152, paper by D.G. Martin, The thermal expansion of solid UO_2 and (U, Pu) – A review and recommendations, pp. 94–101, Fig. 2 [10], Copyright (1988), with permission from Elsevier Science.

3.2. Enthalpy

Fink [11] has suggested that the enthalpy of UO_2 below the Bredig phase transition [12] at 2670 K may be approximated by the following expression:

$$H_T^0 - H_{298.15}^0(\text{J mol}^{-1}) = C_1\theta[(\exp(\theta/T)-1)^{-1} - (\exp(\theta/298.15)-1)^{-1}] + C_2[T^2 - (298.15)^2] + C_3 k_B (T\exp(-E_a/k_BT) - 298.15\exp(-E_a/(k_B\ 298.15)), \quad (3.4)$$

where T is in K and k_B is the Boltzmann constant equal to 8.6144×10^{-5} eV K^{-1}. The three terms in (3.4) represent contributions due to phonons, thermal expansion and electrons respectively. The values used for the parameters θ, C_1, C_2, C_3 and E_a are given in Table 2.

Equation (3.4) is constrained by the conditions

$$H_T^0 - H_{298.15}^0 = 0|_T = 298.15\ \text{K} \quad (3.5)$$

and

$$\left(\frac{\partial H}{\partial T}\right)_P\Big|_{T=298.15\ \text{K}} = C_p(298.15\ \text{K}) = 63.6\ \text{J mol}^{-1}\ \text{K}^{-1}. \quad (3.6)$$

The above value for the heat capacity at 298.15 K is from experimental measurements by Huntzicker and Westrum [13].

Above the phase transition of 2670 K and below the melting point of 3120 K, the data were fitted to the linear equation

$$H_T^0 - H_{298.15}^0\ (\text{J mol}^{-1}) = 167.04T - 218342. \quad (3.7)$$

The agreement between approximations (3.4) and (3.7) with experimental data is illustrated by Fig. 8. Note that there is a slight descrepancy between the estimates of the temperature of the Bredig transition by different authors. For example, Gotta and Philipponeau [14] estimated it as 2610 K, but this seems to have little effect on the final result.

3.3. Heat capacity

The value of specific heat capacity C_p can be obtained directly from the value of the enthalpy based on the equation

$$C_p = \frac{\partial H}{\partial T} \quad (3.8)$$

by differentiating Eqs. (3.4) and (3.7), as suggested by Fink [11], which gives

$$C_p\ (\text{J mol}^{-1}\ \text{K}^{-1}) = \frac{C_1\theta^2\exp(\theta/T)}{T^2(\exp(\theta/T)-1)^2} + 2C_2T + C_3k_B\exp(-E_a/k_BT) \times\left(1+\frac{E_a}{k_BT}\right) \quad (3.9)$$

at $T < 2670$ K and

$$C_p\ (\text{J mol}^{-1}\ \text{K}^{-1}) = 167.04 \quad (3.10)$$

at $2670\ \text{K} \leqslant T \leqslant 3120$ K.

The agreement between experimental data and the predictions of (3.9) at temperatures below 1000 K is illustrated in Fig. 9. At higher temperatures, however,

Table 2

θ (K)	C_1 (J mol^{-1} K^{-1})	C_2 (J mol^{-1} K^{-2})	C_3 (J mol^{-1} eV^{-1})	E_a (eV)
516.12	78.215	3.8609×10^{-3}	3.4250×10^{8}	1.9105

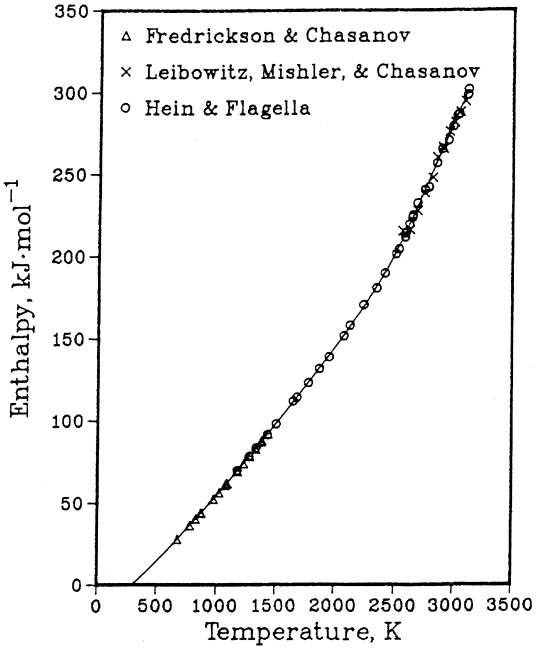

Fig. 8. Measured values of $H_T^0 - H_{298.15}^0$ for UO_2 and the equations (3.4) and (3.7) to fit these data This figure is a reproduction of Fig. 1 by Fink [11] with permission from Plenum Publishing Corporation and the author.

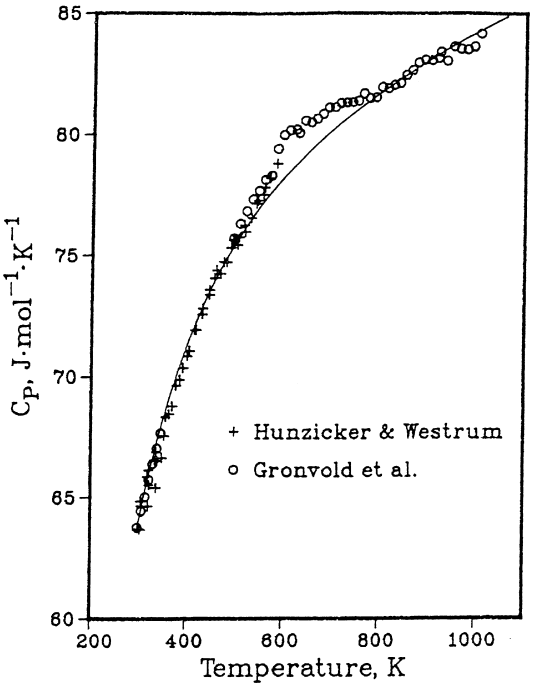

Fig. 9. Measured values of C_p for UO_2 and and those predicted by Equations (3.9) and (3.10). This figure is a reproduction of Fig. 2 by Fink [11] with permission from Plenum Publishing Corporation and the author.

and especially beyond the Bredig transition temperature, data appear to be not very reliable, so that the recommended values of C_p may vary by up to 35% [14]. This is illustrated in Fig. 10, taken from [14], where approximations suggested by Fink [11] (Eqs. (3.9) and (3.10)), Hyland and Ohse [15], and Bredig [12] are compared against experimental data (the meaning of the plots KS and HF have not been identified in the paper).

As was emphasised by Hyland and Ohse [15], insufficient data in the 500 K range up to the melting point means that it is impossible to establish any statistically significant dependence of C_p on temperature rather than a constant ($= 161 \pm 4$ J mol^{-1} K^{-1}, which is slightly lower than that predicted by Fink [11]). For molten UO_2 the situation appears to be even more ambiguous. Hyland and Ohse [15] suggested that a constant value of

$$C_p = 138 \pm 4 \text{ J mol}^{-1} \text{ K}^{-1} \tag{3.11}$$

is used in this case.

3.4. Thermal conductivity

Gotta and Philipponneau [14] suggested that the thermal conductivity λ is estimated from the equation

$$\lambda = a\rho C_p, \tag{3.12}$$

where a is the thermal diffusivity, ρ is the density. Since, however, no indications on the values of a are given in their short paper, Eq. (3.12) appears to be of little practical importance at the moment. On the other hand,

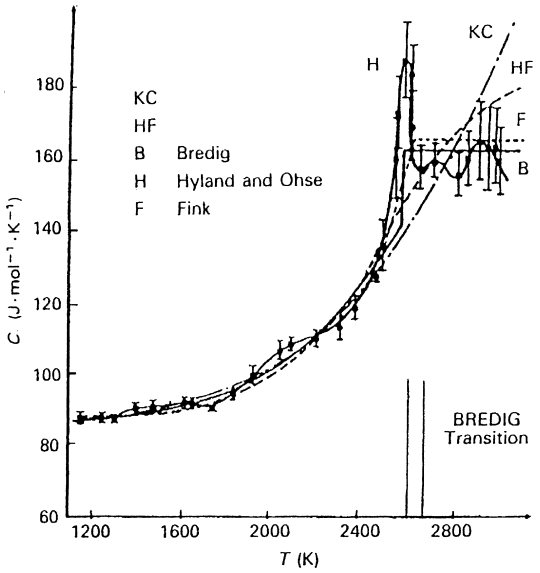

Fig. 10. Measured values of C_p for UO_2 as reported by different authors. This figure is a partial reproduction of Fig. 1 by Gotta and Philipponneau [14] with permission from American Nuclear Society.

Pillai and George [16] suggested that λ be approximated as

$$\lambda = (A + BT)^{-1}, \tag{3.13}$$

where

$$A = 2.997 \times 10^{-2}\ \mathrm{W^{-1}\ m\ K},\quad B = 2.414 \times 10^{-4}\ \mathrm{W^{-1}\ m}. \tag{3.14}$$

Eq. (3.13) was compared with experimental data corrected for porosity (using Loeb's equation: see Francl and Kingery [17]). The result of this comparison is shown in Fig. 11 [16]. Approximation (3.13) is expected to be acceptable at temperatures below 1600 K.

A more accurate relation between temperature (in K) and thermal conductivity (in $\mathrm{W\ m^{-1}\ K^{-1}}$) was suggested by Harding and Martin [18] and recommended by INSC

$$\lambda = \left(0.0375 + 2.165 \times 10^{-4}\ T\right)^{-1} + \frac{4.715 \times 10^{9}}{T^{2}} \times \exp\left(-16361/T\right). \tag{3.15}$$

The effects of porosity on thermal conductivity is discussed by Wagh [19], while Hayes and Peddicord [20] discussed the radiative heat transfer in porous uranium dioxide (for a general review of radiative heat transfer in porous media readers are referred to Kiviany and Singh [21]. A detailed discussion of these papers is beyond the scope of this review.

We will not discuss other physical properties of uranium dioxide which do not seem to be directly relevant to the problem under consideration (for discussion of the lattice structure and vibrational frequencies of UO_2 see Kozlov et al. [22]).

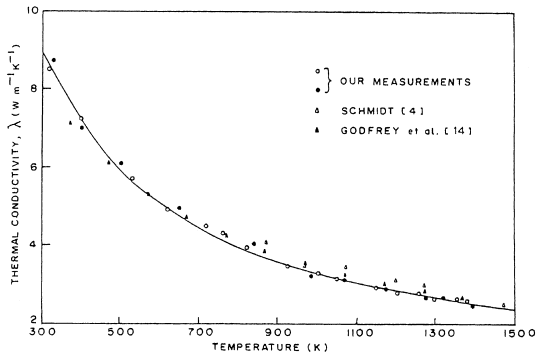

Fig. 11. Thermal conductivity of UO_2 as calculated from equation (3.13) plotted against absolute temperature, along with literature values. Reprinted from Journal of Nuclear Materials, vol. 200, paper by C.G.S. Pillai, A.M. George, Thermal conductivity of uranium dioxide, pages 78–81, Fig. 1 [16], Copyright (1993), with permission from Elsevier Science.

4. Physical properties of UF_6

4.1. Phase diagram

The phase diagram of UF_6 is schematically shown in Fig. 12 [23]. The sublimation point at atmospheric pressure is at $T = 56.2$°C, while melting occurs in the range 64.5–64.8°C [9] with the triple point at $T = 64.02$°C and $p = 1.497$ atm. Since we are mainly interested in pressures close to 1 atm, the discussion of the critical point ($T = 230.2$°C; pressure= 45.5 atm) will be beyond this review.

4.2. Density

The density changes with temperature for the solid phase can be described by the following equation [23]:

$$\rho_s = 5194 - 5.168\,T\ \ \mathrm{kg/m^3} \tag{4.1}$$

for

$$0^{\circ}\mathrm{C} \leqslant T \leqslant 64^{\circ}\mathrm{C}.$$

In the liquid state the density of UF_6 varies in a non-linear fashion and can be summarised by the following equation [23]:

$$\rho_l = 1670 + 152.03\,(T_c - T)^{0.5}\ \mathrm{kg/m^3}, \tag{4.2}$$

where $T_c = 230.2$°C, which is accurate close to triple point, and

$$\rho_l = 2084.3 - 3.1\,T + 371\,(T_c - T)^{0.3045}\ \mathrm{kg/m^3}, \tag{4.3}$$

which is more accurate close to the critical point. Note that T in Eqs. (4.1)–(4.3) is measured in °C.

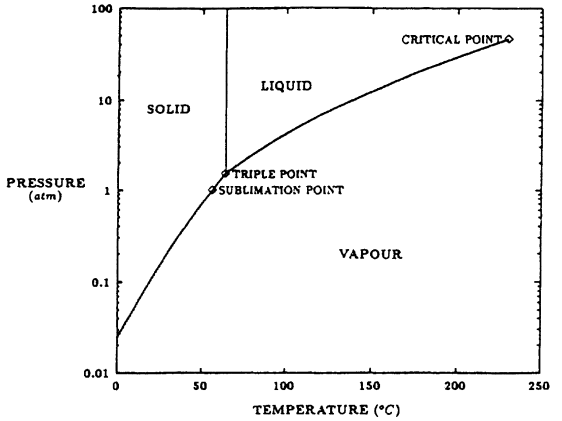

Fig. 12. UF_6 phase diagram. Reprinted from Nuclear Engineering and Design, vol. 140, paper by Lewis et al., An adaptive finite element model for the behaviour of uranium hexafluoride filled container in a fire, pp. 229–250. Copyright (1993).

In the vapour phase, the density of UF_6 can be described according to an equation which is similar in form to the ideal gas law [23]

$$\rho_v = \frac{4291\,p}{T(1 - 1.3769 \times 10^6 p/T^3)}\ \mathrm{kg/m^3}, \tag{4.4}$$

where p is in atm, T is in K. (This expression was based on experimental studies by Weinstock and Crist [24] and Weinstock et al. [24].)

This expression for ρ_v for vapour can be approximated in a simpler way [26]:

$$\rho_v = \frac{4291\,p}{T}(1 + 1.2328 \times 10^6 p/T^3)\ \mathrm{kg/m^3}, \tag{4.5}$$

Comparing (4.1) and (4.2) we can see that during the change from solid to liquid at 64°C a volume expansion of 25.36% takes place (density changes from 4863.25 kg/m^3 (solid) to 3629.95 kg/m^3 (liquid)).

4.3. Heat capacity and enthalpy

The heat capacity and enthalpy of both solid and liquid UF_6 have been studied experimentally by Brickwedde et al. [27]. Their results are summarized in Fig. 13. Lewis et al. [23] presented essentially the same data for C_p but with units J/(kg C), remembering that molecular weight of UF_6 is equal to 0.352 kg/mol (see their Table 3). Values of C_p for UF_6 gas were calculated by Bigeleisen et al. [28] from spectroscopic data. In Table 3 their results are reproduced in units of J/(mol K) (original data were presented in units of cal/(mol K) (1 J = 0.239 cal).

As indicated by Bigeleisen et al. [28] these data coincide to within an accuracy better than 0.7% with experimental data in the range of temperatures from 273 to 358 K. Essentially the same values but in J/(kg °C) are given by Lewis et al. [23] (see Table 4).

Although we could not find any data at temperatures beyond 1000 K, it seems reasonable to assume that

$$C_p\ (T > 1000\ \mathrm{K}) \approx C_p\ (T = 1000\ \mathrm{K})$$

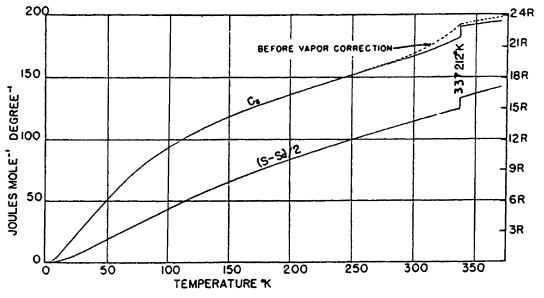

Fig. 13. Molar heat capacity and entropy of UF_6. This figure is a reproduction of Fig. 5 by Brickwedde et al. [27] with permission from American Physical Society.

Table 3
Values of C_p from specroscopic data (based on Table 4 of Bigeleisen et al. [28])

T (K)	C_p (J/(mol K))
273	126.1
298	129.7
323	132.8
348	135.5
373	137.8
400	140.0
500	145.6
750	152.1
1000	154.6

Table 4
Adopted conductivity of UF_6 material [23]

Phases	T (°C)	Thermal conductivity (W/(m °C))
Solid	35	0.058
	45	0.849
	55	1.128
	65	2.616
Liquid	75	290.7
	85	290.7
	95	290.7
	105	290.7
	115	290.7
Vapour	0	2.1385
	38	2.4798
	50	2.5876
	100	3.0366
	150	3.4857
	200	3.8920

since the dependence of C_p on T at T close to $T = 1000$ K is very weak (see Table 3).

4.4. Thermal conductivity

Results of different experimental measurements of thermal conductivity (available from unpublished technical reports) have been summarized by Lewis et al. [23] and are presented in Table 4.

When estimating the thermal conductivity of the liquid phase, the effect of convection was treated as an equivalent heat conduction. For the vapour phase the following experimentally obtained expression was used:

$$\lambda_v = 6.11\ (1 + 0.0042\,T) \times 10^{-3}\,\frac{\mathrm{W}}{\mathrm{m\ ^\circ C}}. \tag{4.6}$$

(This expression is most accurate in the range 0–100°C.)

Following an approximate estimation of the radiation/convection in the vapour domain, an equivalent conductivity for vapour as shown in Table 4 is 350 times greater than that defined by (4.6). This assumption was

rather speculative and is appropriate to a particular problem discussed by Lewis et al. [23] (see Section 5 in this paper) and might need to be modified for other problems.

We could not find any data on thermal conductivity at temperatures above 200°C. However, if these temperatures are about or larger than 1500°C, then one can assume that the effects of thermal conductivity proper can be ignored when compared with the radiation heat transfer. Moreover, at these high temperatures the medium can be considered as optically thick so that the Roosseland approximation can be applied (see Siegel and Howell [29] for details). This approximation allows us to present the total thermal conductivity as

$$\lambda_{\mathrm{v}} = \lambda_{\mathrm{v0}} + \lambda_{\mathrm{vR}}, \tag{4.7}$$

where λ_{v0} is the thermal conductivity proper (e.g., defined by Eq. (4.6)), the contribution of which can be ignored in most cases, and

$$\lambda_{\mathrm{vR}} = \frac{16\sigma T^3}{3a_{\mathrm{R}}} \tag{4.8}$$

is the radiative thermal conductivity, where

$$\sigma = 5.67 \times 10^{-8}\ \frac{\mathrm{W}}{\mathrm{m^2\ K}} \tag{4.9}$$

is the Stefan–Boltzmann constant, a_{R} is the mean absorption coefficient of the thermal radiation.

Values of $\lambda_{\mathrm{g}} \equiv \lambda_{\mathrm{vR}}$ for UF_6 at rather high temperatures and pressures, estimated from observations (curve *a*) and calculated (curve *b*) are presented in Fig. 14 (Dobkin and Son [30]). As one can see from this figure, λ_{vR} is approximately proportional to pressure. Extrapolating these data to atmospheric pressure we can expect that

$$\lambda_{\mathrm{vR}}\,(p = 0.1\mathrm{MPa},\ T = 1000^{\circ}\mathrm{C}) \approx 300\ \frac{\mathrm{W}}{\mathrm{m^2\ K}}. \tag{4.10}$$

Other approaches to the problem of thermal radiation in a high temperature ($> 10^4$ K) media have been discussed by Ernst et al. [31] and Zhang et al. [32].

4.5. Vapour pressure of UF_6

The complexity of the molecules of UF_6 might make the corrections to the gas law important. Magnuson [33] suggested that the equation of state for UF_6 may be written as

$$pV = RT + bp, \tag{4.11}$$

where

$$b = -\frac{3.2 \times 10^3}{T^2}\ \frac{\mathrm{cal}}{\mathrm{mol\,(mm\,Hg)}}, \tag{4.12}$$

T is in K.

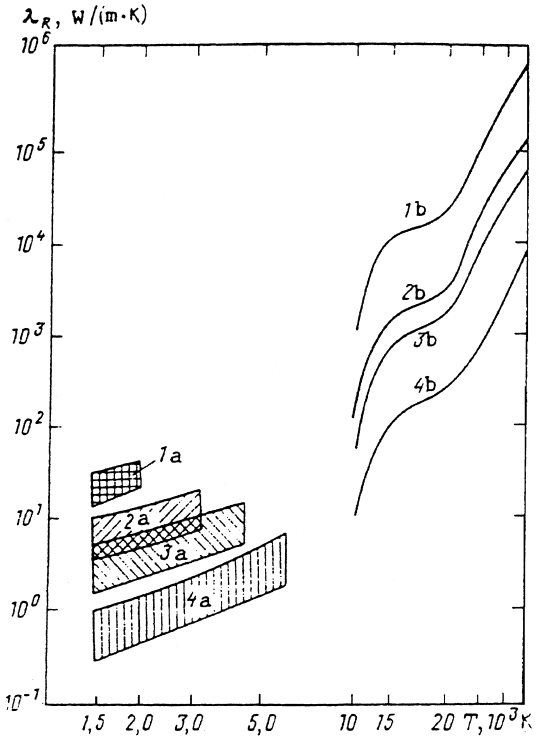

Fig. 14. Radiative thermal conductivity for uranium hexafluoride as a function of temperature for various pressures p: Curve 1 corresponds to $p = 1$ MPa. curve 2 corresponds to $p = 5$ MPa; curve 3 corresponds to $p = 10$ MPa; curve 4 corresponds to $p = 50$ MPa. This figure is a reproduction of Fig. 3 by Dobkin and Son [30] with permission from Plenum Publishing Corporation.

There is some ambiguity about the exact value of b used in Eq. (4.11). Suggested values of b varied from

$$b = -\frac{3.1 \times 10^3}{T^2}\ \frac{\mathrm{cal}}{\mathrm{mol\,(mm\,Hg)}}$$

to

$$b = -\frac{3.6 \times 10^3}{T^2}\ \frac{\mathrm{cal}}{\mathrm{mol\,(mm\,Hg)}}$$

(see Weinstock et al. [25]).

4.6. Electronic structure and chemical bonding

The virtual absence of a dipole moment and the octahedral structure of UF_6 molecules was recognized almost 50 years ago [28]. Since that time the electronic structure and chemical bonding of UF_6 have been studied in numerous papers. Referring to the most recent publications we can mention the paper by Armstrong et al. [34] where the effects of multiphoton ionization were studied experimentally and in a series of

theoretical papers by Onoe et al. [35–38]. A detailed discussion of these papers is beyond the scope of the present review. Although these studies are unlikely to have an immediate practical application to fluorination of UO_2 they might be able to contribute to our in-depth understanding of the underlying processes.

5. Physical properties of F_2 and Ar

5.1. General properties

Melting points of F_2 and Ar are -223°C and -189.2°C, respectively; their boiling points are -187°C and -185.7°C, respectively [8].[1] Hence, in most practical applications both substances can be treated as gases for which the equation of state for the ideal gas can be assumed accurate (for the discussion about other equations of state see Reid et al. [39]). Heat capacities C_p of F_2 and F (in cal/mol K) are given in [6]. The value of C_p for Ar can be expected to be reasonably close to that of F (the reference is not available at the moment).

From kinetic theory the coefficients of laminar viscosity of F_2 and Ar can be written as [40]

$$\mu = 2.6693 \times 10^{-6} \frac{\sqrt{MT}}{\sigma_M^2 \Omega_\mu} \left(\frac{\text{kg}}{\text{m s}} \right), \tag{5.1}$$

where M is the molecular weight (M for F_2 is equal to 38.00 kg/k mol; M for Ar is equal to 39.94 kg/k mol), T is temperature in K, σ_M is the characteristic molecular diameter measured in nm and Ω_μ is a slowly varying function of the dimensionless parameter $k_B T/\epsilon_M$ (k_B is the Boltzmann constant, ϵ_M is the characteristic energy of interaction between the molecules, or, in other words, the maximal energy of attraction between a pair of molecules).

The values of σ_M and ϵ_M/k_B for F_2 and Ar are shown in Table 5 [40]. The corresponding values of Ω_μ are given by Bird et al. [40].

The coefficients of thermal conductivity of F_2 and Ar can be estimated based on the semi-empirical Eucken formula [40]

$$\kappa = \left(C_p + \frac{5}{4} R_G \right) \frac{\mu}{M} \left[\frac{\text{W}}{\text{m K}} \right], \tag{5.2}$$

where μ is viscosity determined by (5.1), C_p is the specific heat, M is the molecular weight, the universal gas constant R_G is expressed in J/(kg mol K).

[1] The referee of the paper drew our attention to the fact that the data for F_2 given in [8] are not reliable and suggested to take -219°C and -188.1°C for melting and boiling points of F_2, respectively.

Table 5

Gas	σ_M (nm)	ϵ_M/k_B (K^{-1})
F_2	3.653	112.0
Ar	3.418	124.0

In the case of a mixture of gases the Wilke semi-empirical formula [41] can be used

$$\mu_\Sigma = \sum_{i=1}^{3} \frac{\mu_i}{1 + \sum_{j=1(i\neq j)}^{3} y_j \Phi_{ij}/y_i}, \tag{5.3}$$

where y_i are mole fractions of particular species, indices i and j refer to different species (in our case F_2 (i or j are equal to 1) and Ar (i or j are equal to 2)),

$$\Phi_{ij} = \frac{\left[1 + (\mu_i/\mu_j)^{1/2} (M_j/M_i)^{1/4} \right]^2}{\left[8(1 + M_i/M_j) \right]^{1/2}}. \tag{5.4}$$

For the calculation of the coefficient of thermal conductivity for the given mixture of gases we use the Mason and Saxena semi-empirical formula [42]

$$\kappa_\Sigma = \sum_{i=1}^{3} \frac{\kappa_i}{1 + 1.065 \sum_{j=1(i\neq j)}^{3} y_j \Phi_{ij}/y_i}, \tag{5.5}$$

where y_i, Φ_{ij} and the meaning of indices i and j are the same as in (5.4).

Computations of a specific heat of the mixture can be based on the following well known expression

$$\overline{c}_p = \frac{\sum_{i=1}^{3} y_i c_{pi}}{\sum_{i=1}^{3} y_i M_i}. \tag{5.6}$$

Expressions for viscosity and thermal conductivity presented in this section are valid in a low density limit which is applicable for the case when the pressure is less or about 1 atm [40].

Note that in most realistic cases the values of μ_Σ and κ_Σ determined by (5.3) and (5.5) are dominated by their turbulent counterparts. Discussion of the turbulence models is beyond the scope of the present paper (see e.g. [43]).

5.2. Collision cross-sections of electrons with F_2

Collision cross-sections of electrons with the molecules of F_2 have been recently summarized in the reviews by Hayashi and Nimura [44]. The cross-sections obtained from different sources are presented in Fig. 15.

The momentum cross-sections q_m were assumed to be equal to the total cross-sections at energies below 14 eV. At greater energies q_m for F_2 was assumed to be equal to q_m for N_2. The values of the vibrational excitation cross-section, q_v (threshold 0.11 eV) were taken from the theoretical paper by Hall [46]. The curves for q_{e1} to q_{e4} show

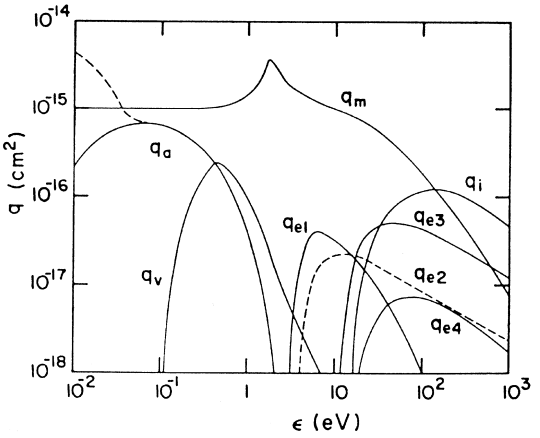

Fig. 15. Cross-sections of electrons in F_2 summarized by Hayashi and Nimura [44]. q_m refers to momentum cross-section, q_a refers to attachment cross-section, q_v refers to vibrational excitation cross-section, q_i refers to ionization cross-section, q_{e1} to q_{e4} refer to excitation cross-sections of $a^3\Pi_u$, $A^1\Pi_u$, $C^1\Sigma_u^+$ and $H^1\Pi_u$ levels, respectively. This figure is a reproduction of Fig. 1 by Hayashi and Nimura [44] with permission from American Physical Society.

the excitation cross-sections of $a^3\Pi_u$ (threshold 3.16 eV), $A^1\Pi_u$ (threshold 4.34 eV), $C^1\Sigma_u^+$ (threshold 11.57 eV), and $H^1\Pi_u$ (threshold 13.08 eV), levels respectively. Note that Hayashi and Nimura [44] did not know any theoretical or experimental data referring to the level $A^1\Pi_u$ and they had to use indirect evidence to present the curve for q_{e2}. The ionization cross-section q_i was taken from the measurements by Stevie and Vasile [47] in the energy range from threshold 15.69 eV to about 100 eV, and these data were extrapolated smoothly to higher energies. For the attachment cross-section q_a the theoretical results of Hazi et al. [48] were used. These were slightly different from the experimental results reported by Chantry [49] (dotted continuation of the q_a plot at energies below 0.1 eV). There are some arguments that Chantry's results are more adequate [45]. Note that in the case of F_2, attachment has a dissociative nature

$$F_2 + e^- \rightarrow F^- + F. \tag{5.7}$$

For given values of E/N (ratio of electric field to particle density) the cross-sections presented in Fig. 15 can allow us to compute the electron energy distribution function and the corresponding transport coefficients [50–57].

For more refined recent theoretical and experimental analyses of F_2 molecules see [58–64].

5.3. Collision cross-sections of electrons with Ar

Momentum transfer cross-sections for argon reported by Frost and Phelps [65] are still considered as the most reliable ones [66]. The plot of these cross-sections versus energy is shown in Fig. 16.[2] The solid curve shows the values recommended by Frost and Phelps [65] and this is compared with the results reported by other authors both for the momentum and total cross-sections.

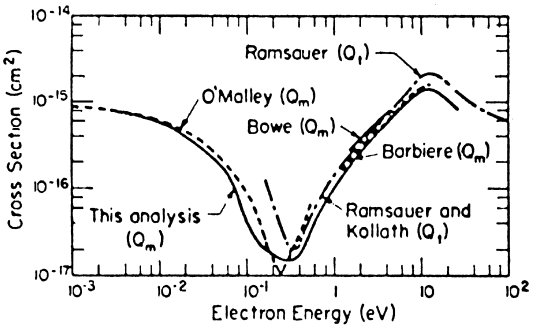

Fig. 16. Momentum transfer, Q_m, and total, Q_t, cross-sections of electrons in argon suggested by different authors and summarized by Frost and Phelps [65]. The solid curve gives the final momentum transfer cross section used by Frost and Phelps [65]. This figure is a reproduction of Fig. 4 by Frost and Phelps [65] with permission from American Physical Society and the authors.

Results of measurements and theoretical calculations of inelastic electron impact cross-sections for argon have been reported by many authors [67–72]. A critical review of most of these papers is given by Fereira and Loureiro [66]. We are interested in total inelastic electron cross-sections rather than cross-sections referring to individual levels. Plots of these cross-sections recommended by different authors is presented in Fig. 17. Except for the curve based on the results by Eggarter [68], all the curves seem to be rather close to each other. The solid curve is the one recommended by Fereira and Loureiro [66]. For the results of measurements of the superelastic collision cross-section of argon metastable atoms see [73].

6. Uranium–fluorine plasma

The properties of UF_6 or decomposition of UF_6 at high temperatures were considered by Krascella [74], Roman [75], and Tumanov and Tsirel'nikov [76–78]. The latter three papers reported the results of experiments with RF discharges in a mixture of Ar and UF_6 with possible addition of water. Without describing all technical details of the experiments reported by Tumanov and Tsirel'nikov [76–78] we just mention that the

[2] Dr A.V. Phelps drew our attention to the fact that more recent cross-section data for Ar and other gases are available at http://jilawww.colorado.edu/ on the atomic physics page under collision data.

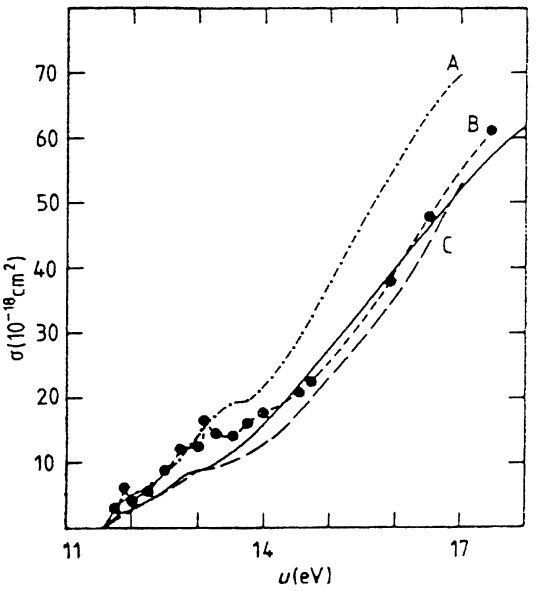

Fig. 17. Total electron excitation cross-section for argon. Solid curve is that recommended by Ferreira and Loureiro [66], curve A is that recommended by Eggarter [68], curve B is that recommended by Sprecht et al. [70], curve C is that recommended by Jacob and Mangano [69]. This figure is a reproduction of Fig. 3 by Ferreira and Loureiro [66] with permission from the Institute of Physics (UK) and the authors.

power level of their discharge varied up to 85 kW, and the pressure in a discharge chamber to 10^6 Pa, the flow rate of UF_6 to 21 g/s. Mass flowrate of argon was 2.58 g/s, ratio of masses UF_6/Ar was 0.012. Frequency of a discharge was 5.42 MHz; discharge diameter 2.8 cm.

Firstly, it was shown that part of the UF_6 molecules decompose so that atoms of U appear in the discharge. Secondly, it was noticed that the wall of the quartz discharge pipe was coated with UO_2F_2. The formation of this deposit might have been caused by the interaction of UF_6 with the material of the quartz pipe:

$$UF_6 + SiO_2 \rightarrow UO_2F_2 + SiF_4. \quad (6.1)$$

This means that the reaction almost opposite to (2.2) takes place.

In the presence of hydrogen, UF_6 and UF_5 become thermodynamically unstable:

$$UF_6 \rightarrow UF_5 + F, \quad (6.2)$$

$$UF_5 \rightarrow UF_4 + F. \quad (6.3)$$

Without discussing all other possible chemical reactions in the uranium–fluorine–hydrogen–oxygen plasma under consideration we just show in Fig. 18 (Tumanov and Tsirel'nikov [77]) a number of moulds of different components as the function of temperature. As can be

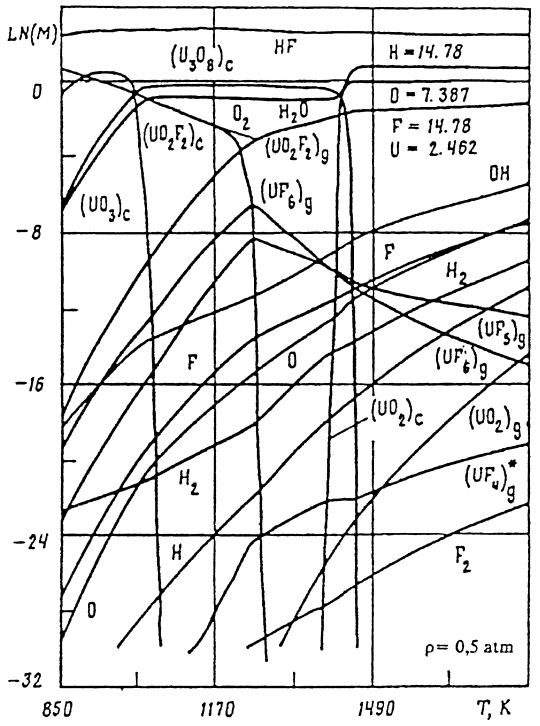

Fig. 18. Dependence of the number of moulds of components of U–F–H–O plasma on temperature for the mixture of UF_6 + $3H_2$) at H = 14.78, O = 7.387, F = 14.78 and U = 2.462 mol/kg. See Tumanov and Tsirel'nikov [77] for details. This figure is a reproduction of Fig. 1 by Tumanov and Tsirel'nikov [77] with permission from Riecansky Science Publishing.

seen from this figure, the concentration of UF_6 increases with temperature up to about 1200 K and decreases at higher temperatures. Hence, the optimum conditions for the production of UF_6 in this plasma could be expected at temperatures below 1200 K.

Referring to other plasmas containing fluorine atoms we can mention a reduction of concentration of composite molecules with increasing temperature in C–N–F plasma [79] and reduction of SF_6 with temperature in SF_6–Cu mixtures [80]. Among other relevant references referring to plasma chemistry we can mention [81–83].

7. Particulates dynamics

If the reactions (2.1) and (2.2) are expected to take place with aerosols or powder of UO_2 then the problem of particulates movement in the medium and exchange of heat between particulates and the medium needs to be considered. In the case of neutral gas, particulates trajectories were considered by Morsi and Alexander [84]. Simple analytical expressions derived by these authors

appeared to be very useful for numerical coding and have been used by Sazhin and Jeapes [1].

The case of particulate dynamics in DC discharges was recently discussed by Winske and Jones [85]. Li Ming and Chen Yunming [86] attempted to take into account the effects of nonspherical particles on the particulate-plasma heat transfer. In the case of very fine aerosols we come accross the general problem of the dynamics of a dusty plasma [87–99].

8. Conclusions

1. There exist strong indications that the maximum rate of fluorination of uranium dioxide can be achieved at temperatures above 540°C which supports a study of this process at these elevated temperatures.
2. Basic physical properties of uranium hexafluoride, fluorine and uranium dioxide are available from the literature and are summarised in this paper. These properties can be used in preliminary computer simulations of the fluorination of uranium dioxide at temperatures below 540°C, where the reaction rate is known.
3. Cross-sections of electron collisions with argon and fluorine are well documented in the literature, and can be used for self-consistent simulations of transport properties of argon–fluorine plasma. However, there seem to be no reliable reports on similar cross-sections for uranium hexafluoride, which makes it rather difficult to quantify the transport properties of a uranium–fluorine plasma.

Acknowledgements

Authors are grateful to BNFL for financial support. Elsevier Science BV, Americal Chemical Society, Plenum Publishing Corporation, American Nuclear Society, American Physical Society, Riecansky Science Publishing, Elsevier Science SA, A.V. Phelps, J.K. Fink and C.M. Ferreira are acknowledged for their permissions to reproduce figures from the original papers.

References

[1] S.S. Sazhin, A.P. Jeapes, J. Nucl. Mater. 249 (1997) 207.
[2] M. Iwasaki, J. Nucl. Mater. 25 (1968) 216.
[3] T. Sakurai, J. Phys. Chem. 78 (12) (1974) 1140.
[4] T. Yahata, M. Iwasaki, J. Inorg. Nucl. Chem. 26 (1964) 1863.
[5] T. Sakurai, JAERI (1976) 1243.
[6] K.K. Kuo, Principles of Combustion, Wiley, New York, 1986.
[7] B.F. Magnussen, B.H. Hjertager, On mathematical models of turbulent combustion with special emphasis on soot formation and combustion, in: 16th Symposium (International) on Combustion, Cambridge, MA, 1976, p. 719–729.
[8] R.H. Perry, D Green, Perry's Chemical Engineers' Handbook (6th ed.), McGraw–Hill, New York, 1984.
[9] CRC Handbook of Chemistry and Physics, (52nd ed.), CRC, Boca Raton, FL, 1972.
[10] D.G. Martin, J. Nucl. Mater. 152 (1988) 94.
[11] J.K. Fink, Int. J. Thermophys. 3 (2) (1982) 165.
[12] M.A. Bredig, The order–disorder (lambda) transition in uranium dioxide and other solids of the fluorite type structure, Colloques Internationaux C.N.R.S. No. 205, 1971, p. 183–191.
[13] J.J. Huntzicker, E.F. Westrum Jr., J. Chem. Thermodynam. 3 (1) (1971) 61.
[14] M.J. Gotta, Y. Philipponneaux, Trans. Am. Nucl. Soc. 66 (1992) 179.
[15] G.J. Hyland, R.W. Ohse, J. Nucl. Mater. 140 (1986) 149.
[16] C.G.S. Pillai, A.M. George, J. Nucl. Mater. 200 (1993) 78.
[17] J. Francl, W.D. Kingery, J. Am. Ceramic Soc. – Loeb 37 (2) (1954) 99.
[18] J.H. Harding, D.G. Martin, J. Nucl. Mater. 166 (1989) 223.
[19] A.S. Wagh, J. Mater. Sci. 28 (1993) 3715.
[20] S.L. Hayes, K.L. Peddicord, J. Nucl. Mater. 202 (1993) 87.
[21] M. Kaviany, B.P. Singh, Adv. Heat Transfer 23 (1993) 133.
[22] Zh.A. Kozlov, I. Padureanu, S. Rapeanu, G. Rotarescu, V.A. Semenov, Phys. Solid State 35 (7) (1993) 991.
[23] R.W. Lewis, Y. Zheng, D.T. Gethin, Nucl. Eng. Design 140 (1993) 229.
[24] B. Weinstock, R.H. Crist, J. Chem. Phys. 16 (5) (1948) 436.
[25] B. Weinstock, E.E. Weaver, J.G. Malm, J. Inorg. Nucl. Chem. 11 (1959) 104.
[26] J.F. Masi, J. Chem. Phys. 17 (9) (1949) 755.
[27] F.G. Brickwedde, H.J. Hoge, R.B. Scott, J. Chem. Phys. 16 (5) (1948) 429.
[28] J. Bigeleisen, M.G. Mayer, P.C. Stevenson, J. Turkevich, J. Chem. Phys. 16 (5) (1948) 442.
[29] R. Siegel, J.R. Howell, Thermal Radiation Heat Transfer, Hemisphere, Washington, DC, 1992.
[30] S.V. Dobkin, E.E. Son, High Temp. (USA) 29 (3), (1991) 365.
[31] K.A. Ernst, J.G. Kopainsky, H.H. Maecker, IEEE Trans. Plasma Sci. PS-1 (1973) 3.
[32] J.F. Zhang, M.T.C. Fang, D.B. Newland, J. Phys. D 20 (1987) 368.
[33] D.W. Magnuson, J. Chem. Phys. 24 (2) (1956) 344.
[34] D.P. Armstrong, D.A. Harkins, R.N. Compton, D. Ding, J. Chem. Phys. 100 (1) (1994) 28.
[35] J. Onoe, R. Sekine, K. Takeuchi, H. Nakamatsu, T. Mukoyama, H. Adachi, Chem. Phys. Lett. 217 (1/2) (1994) 61.
[36] J. Onoe, K. Takeuchi, H. Nakamatsu, T. Mukoyama, R. Sekine, H. Adachi, Chem. Phys. Lett. 196 (6) (1992a) 636.
[37] J. Onoe, K. Takeuchi, H. Nakamatsu, T. Mukoyama, R. Sekine, H. Adachi, J. Electron Spectrosc. Related Phenom. 60 (1992b) 29.

[38] J. Onoe, K. Takeuchi, H. Nakamatsu, T. Mukoyama, R. Sekine, B.-I. Kim, H. Adachi, J. Chem. Phys. 99 (9) (1993) 6810.
[39] R.C. Reid, J.M. Prausnitz, T.S. Sherwood, Properties of Gases and Liquids, McGraw–Hill, New York, 1987.
[40] R.B. Bird, W.E. Stewart, E.N. Lightfoot, Transport Phenomena, Wiley, New York, 1960.
[41] C.R. Wilke, J. Chem. Phys. 18 (4) (1950) 517.
[42] E.A. Mason, S.C. Saxena, Phys. Fluids 1 (5) (1958) 361.
[43] P. Bradshaw (Ed.), Turbulence. Springer, Berlin, 1976.
[44] M. Hayashi, T. Nimura, J. Appl. Phys. 54 (9) (1983) 4879.
[45] W.L. Morgan, Plasma Chem. Plasma Process. 12 (4) (1992) 449.
[46] R.J. Hall, J. Chem. Phys. 68 (4) (1978) 1803.
[47] F.A. Stevie, M.J. Vasile, J. Chem. Phys. 74 (9) (1981) 5106.
[48] A.U. Hazi, A.E. Orel, T.N. Rescigno, Phys. Rev. Lett. 46 (14) (1981) 918.
[49] P.J. Chantry, in: E.W. McDaniel, W.L. Nighan (Eds.), Applied Atomic Collisions Physics, vol. 3, Gas lasers, Academic Press, New York, 1982, p. 35.
[50] B.E. Cherrington, Gaseous Elec. Gas Lasers, Oxford, Pergamon, 1979.
[51] W.L. Morgan, B.M. Penetrante, Comp. Phys. Commun. 58 (1990) 127.
[52] M. Makhlouf, S.S. Sazhin, C. Leys, D. Toebaert, P. Wild, Infrared Phys. 34 (5) (1993) 525.
[53] T. Kimura, K. Ohe, Jpn. J. Appl. Phys. 32 (8) (1993) 3601.
[54] S. Sazhin, M. Makhlouf, D. Toebaert, C. Leys, Phys. Lett. A 185 (1994) 99.
[55] H. Sugawara, Y. Sakai, H. Tagashira, J. Phys. D 27 (1994) 90.
[56] Yu.P. Raiser, Gas Discharge Physics, Springer, Berlin, 1991.
[57] W.J. Witteman, The CO_2 Laser, Springer, Berlin , 1987.
[58] M. Kakehata, E. Hashimoto, F. Kannari, M. Obara, Appl. Phys. Lett. 56 (26) (1990) 2599.
[59] M. Kakehata, Y. Ueno, K. Tamura, F. Kannari, J. Appl. Phys. 75 (3) (1994) 1304.
[60] M. Kakehata, C.-H. Yang, Y. Ueno, F. Kannari, Appl. Phys. Lett. 61 (26) (1992) 3089.
[61] M. Kakehata, C.-H. Yang, Y. Ueno, F. Kannari, J. Appl. Phys. 74 (4) (1993) 2241.
[62] B.H. Lengsfield, T.N. Rescigno, Phys. Rev. A 44 (5) (1991) 2913.
[63] K. Kobayashi, N. Kurita, K. Tago, Phys. Rev. B 45 (19) (1992) 11299.
[64] K.A. Peterson, R.A. Kendall, T.H. Dunning Jr., J. Chem. Phys. 99 (12) (1993) 9790.
[65] L.S. Frost, A.V. Phelps, Phys. Rev. 136 (6A) (1964) A1538.
[66] C.M. Fereira, J. Loureiro, J. Phys. D 16 (1983) 1611.
[67] D. Rapp, P. Englander-Golden, J. Chem. Phys. 43 (53) (1965) 1464.
[68] E. Eggarter, J. Chem. Phys. 62 (3) (1975) 833.
[69] J.H. Jacob, J.A. Mangano, Appl. Phys. Lett. 29 (8) (1976) 467.
[70] L.T. Sprecht, S.A. Lawton, T.A. DeTemple, J. Appl. Phys. 51 (1) (1980) 166.
[71] A. Chutjan, D.C. Cartwright, Phys. Rev. A 23 (5) (1981) 2178.
[72] C.M. Fereira, J. Loureiro, A. Ricard, J. Appl. Phys. 57 (1) (1985) 82.
[73] T. Okada, M. Sugawara, Measurement of the superelastic collision cross-section of argon metastable atoms for low energy electrons by means of afterglow technique, in: Proceedings of the 21st International Conference on Phenomena in Ionized Gases, vol. 2 (Bochum: Arbeitsgemeinschaft Plasmaphysik Ruhr–Universität), 1993, p. 19.
[74] N.L. Krascella, The spectral properties of uranium hexafluoride and its thermal decomposition products, in: Plasma Chemical Proceedings, AlChE Symposium 75 (186) (1979) 63.
[75] W.C. Roman, Properties of fluid-dynamically stabilized RF-heated argon/UF_6 plasmas, in: Plasma Chemical Proceedings, AlChE Symposium 75 (186) (1979) 50.
[76] Yu.N. Tumanov, K.V. Tsirel'nikov, Phys. Chem. Mater. Treatment 26 (4) (1992a) 424.
[77] Yu.N. Tumanov, K.V. Tsirel'nikov, Phys. Chem. Mater. Treatment 26 (5) (1992b) 541.
[78] Yu.N. Tumanov, K.V. Tsirel'nikov, Phys. Chem. Mater. Treatment 26 (5) (1992c) 549.
[79] B.R. Bronfin, in: R.F. Baddour, R.S. Timmins (Eds.), The Application of Plasmas to Chemical Processing, Pergamon, 1967, p. 157.
[80] B. Chervy, A. Gleizes, M. Razafinimanana, J. Phys. D: 27 (6) (1994) 1193.
[81] M.P. Freeman, in: J.E. Flinn (Ed.), Engineering, Chemistry, and Use of Plasma Reactors, American Institute of Chemical Engineers, 1971, p. 85.
[82] R.E. Cohen, R.F. Baddour, G.A. Corbin, in: H.V. Boenig (Ed.), Advances in Low-Temperature Plasma Chemistry, Technology, Applications, Technomic Publishing, 1983, p. 317.
[83] A. Rutscher, H.-E. Wagner, in: Proceedings of the 21st International Conference on Phenomena in Ionized Gases, vol. 2, Bochum: Arbeitsgemeinschaft Plasmaphysik Ruhr–Universität, 1993, p. 209.
[84] S.A. Morsi, A.J. Alexander, J. Fluid Mech. 55 (2) (1972) 193.
[85] D. Winske, M.E. Jones, IEEE Trans. Plasma Sci. 22 (4) (1994) 454.
[86] Li Ming, Chen Yunming, IEEE Trans. Plasma Sci. 22 (4) (1994) 97.
[87] R.C. Hazelton, E.J. Yadlovsky, IEEE Trans. Plasma Sci. 22 (2) (1994) 91.
[88] B. Walch, M. Horanyi, S. Robertson, IEEE Trans. Plasma Sci. 22 (2) (1994) 97.
[89] M. Shiratani, T. Fukuzawa, Y. Watanabe, IEEE Trans. Plasma Sci. 22 (2) (1994) 103.
[90] Böhme, W.E. Köhler, Römheld, S. Vepřek, R.J. Seeböck, IEEE Trans. Plasma Sci. 22 (2) (1994) 110.
[91] E. Stoffels, W.W. Stoffels, D. Vender, G.M.W. Kroesen, F.J. deHoog, IEEE Trans. Plasma Sci. 22 (2) (1994) 116.
[92] J.F. O'Hanlon, J. Kang, K. Russell, L. Hong, IEEE Trans. Plasma Sci. 22 (2) (1994) 122.
[93] S.E. Beck, S.M. Collins, J.F. O'Hanlon, IEEE Trans. Plasma Sci. 22 (2) (1994) 128.
[94] I. Alexeff, M. Pace, IEEE Trans. Plasma Sci. 22 (2) (1994) 136.
[95] S.J. Choi, M.J. Kushner, IEEE Trans. Plasma Sci. 22 (2) (1994) 138.

[96] C. Cui, J. Goree, IEEE Trans. Plasma Sci. 22 (2) (1994) 151.
[97] T. Nitter, T.K. Aslaksen, F. Melandso, O. Havnes, IEEE Trans. Plasma Sci. 22 (2) (1994) 159.
[98] S. Barabash, R. Lundin, IEEE Trans. Plasma Sci. 22 (2) (1994) 173.
[99] V.W. Chow, D.A. Mendis, M. Rosenberg, IEEE Trans. Plasma Sci. 22 (2) (1994) 179.